High-quality Ruddlesden-Popper perovskite films based on in situ formed organic spacer cations

Qing, Jian; Kuang, Chaoyang; Wang, Heyong; Wang, Yuming; Liu, Xiao-Ke; Bai, Sai; Li, Mingjie; Sum, Tze Chien; Hu, Zhangjun; Zhang, Wenjing; Gao, Feng

2019

Qing, J., Kuang, C., Wang, H., Wang, Y., Liu, X.-K, Bai, S., . . . Gao, F. (2019). High-quality Ruddlesden-Popper perovskite films based on in situ formed organic spacer cations. Advanced Materials, 31(41), 1904243-. doi:10.1002/adma.201904243

https://hdl.handle.net/10356/139196

https://doi.org/10.1002/adma.201904243

Supporting Information

High-Quality Ruddlesden-Popper Perovskite Films Based on In Situ Formed Organic Spacer Cations

Jian Qing, Chaoyang Kuang, Heyong Wang, Yuming Wang, Xiao-Ke Liu, Sai Bai, Mingjie Li, Tze Chien Sum, Zhangjun Hu, Wenjing Zhang* and Feng Gao**

Dr. J. Qing, Prof. W. Zhang
International Collaborative Laboratory of 2D Materials for Optoelectronics Science and Technology of Ministry of Education, Institute of Microscale Optoelectronics, Shenzhen University, Shenzhen 518060, China.
E-mail: wjzhang@szu.edu.cn

Dr. J. Qing, C. Kuang, H. Wang, Y. Wang, Dr. X.-K Liu, Dr. S. Bai, Dr. Z. Hu, Prof. F. Gao
Department of Physics, Chemistry, and Biology (IFM), Linköping University, Linköping SE-58183, Sweden.
E-mail: xiaoke.liu@liu.se; feng.gao@liu.se

Dr. M. Li, Prof. T. C. Sum
Division of Physics and Applied Physics, School of Physical and Mathematical Sciences, Nanyang Technological University, 21 Nanyang Link, Singapore 637371, Singapore.

Materials: PbI_2 (99.999% trace metals basis), $PbCl_2$ (99.999% trace metals basis), [6,6]-phenyl-C_{61}-butyric acid methylester (PCBM, >99.5%), 2,9-dimethyl-4,7-diphenyl-1,10-phenanthroline (BCP, 96%), chlorobenzene (anhydrous, 99.8%), hydroiodic acid (HI, contains no stabilizer, distilled, 57 wt% in H_2O, 99.99% trace metals basis), phenethylamine ($PENH_2$, ≥99%), ammonium iodide (NH_4I, 99.999% trace metals basis), 2-picolylamine ($PCNH_2$, 99%), butylamine (BNH_2, 99.5%), 2-phenoxyethylamine ($POENH_2$, 98%), 4-methoxyphenethylamine ($MOPENH_2$, ≥98%), 1-naphthalenemethylamine ($NMNH_2$, 97%), dimethyl sulfoxide (DMSO, anhydrous, ≥99%) and dimethylformamide (DMF, anhydrous, 99.8%) were purchased from Sigma-Aldrich. Phenylethylammonium iodide (PEAI) and methylammonium iodide (MAI) were purchased from GreatCell Solar. They were all used as received.

RPP LEDs fabrication and characterization

The control NCPI precursor solution was prepared by dissolving NMAI (0.11 mmol), CsI (0.15 mmol), and PbI_2 (0.1 mmol) in DMF (1 mL). For the HI-, NH_4I-, and MAI-based precursor solutions, NMAI in the control precursor was replaced by equimolar $NMNH_2$ together with HI, NH_4I and MAI, respectively, while keeping the other materials the same. The RPP LEDs are fabricated with the device configuration of ITO/polyethylenimine ethoxylated modified zinc oxide/NCPI RPP/poly(9,9-dioctyl-fluorene-co-N-(4-butylphenyl)diphenylamine) (TFB)/molybdenum oxide (MoO_3)/Ag. A detailed description of the device fabrication can be found elsewhere.[1] Characterizations of the devices were carried out at room temperature in a nitrogen-filled glovebox. Specially, *J-V* characteristics were recorded by Keithley 2400 source meter. Forward-viewing spectral radiant flux was measured by an integrating sphere coupled with a QE65 Pro spectrometer. The EQE and radiance were calculated with the assumption that the LEDs are ideal Lambertian emitters, which are

isotropic, emitting with equal radiance into any solid angle within the forward-viewing hemisphere.

FTPS-EQE Measurement

FTPS-EQE was measured using a Vertex 70 from Bruker Optics, which was equipped with a quartz tungsten halogen lamp, quartz beam-splitter and external detector option. A low-noise current amplifier (SR570) was used to amplify the photocurrent produced on illumination of the devices with light modulated by the Fourier transform infrared spectroscope (FTIR). The output voltage of the current amplifier was fed back into the external detector port of the FTIR to use the FTIR software to collect the photocurrent spectrum.

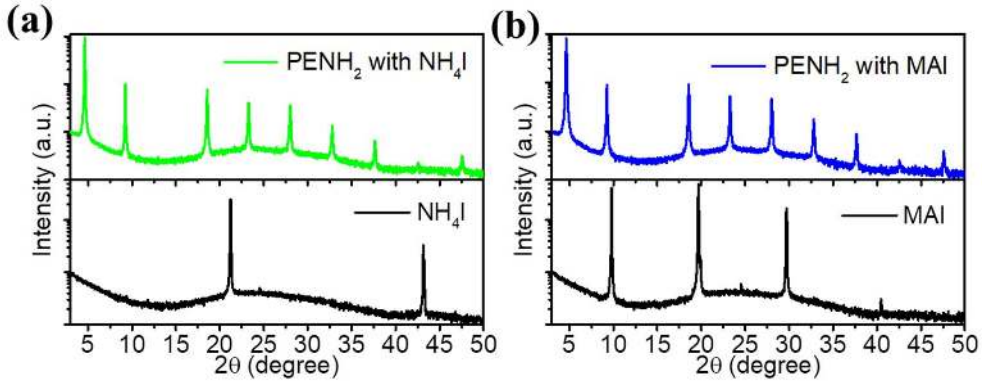

Figure S1. a) XRD patterns for NH_4I and the film obtained from solution of $PENH_2$ with NH_4I. b) XRD patterns for MAI and the film obtained from solution of $PENH_2$ with MAI.

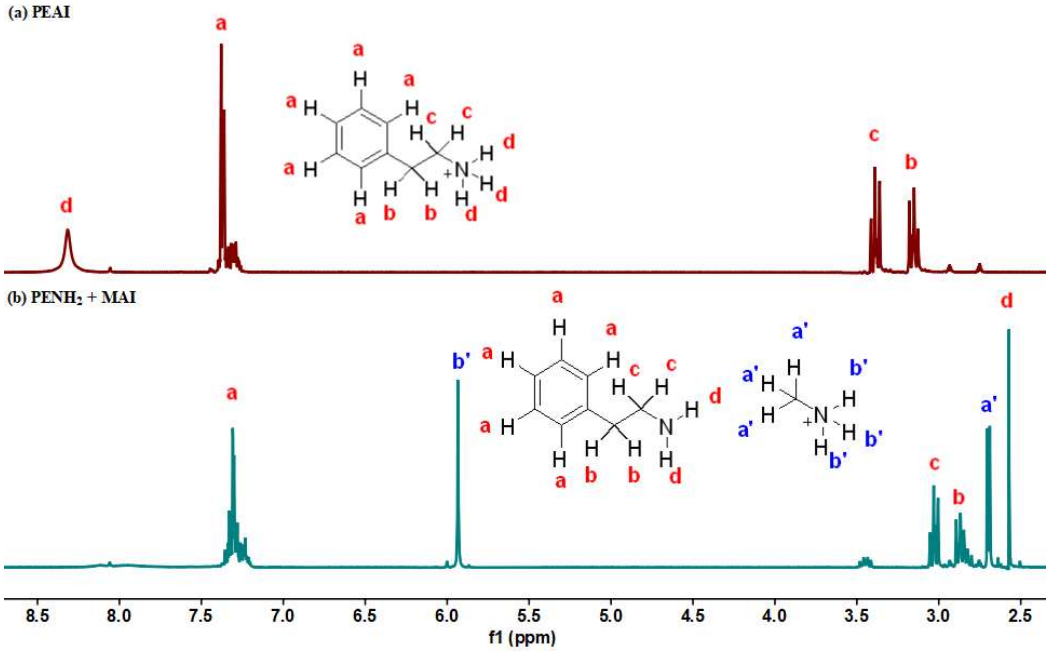

Figure S2. ^{1}H NMR spectra of a) PEAI and b) $PENH_2$ + MAI dissolved in heptadeutero-N,N-dimethylformamide (DMF-d7).

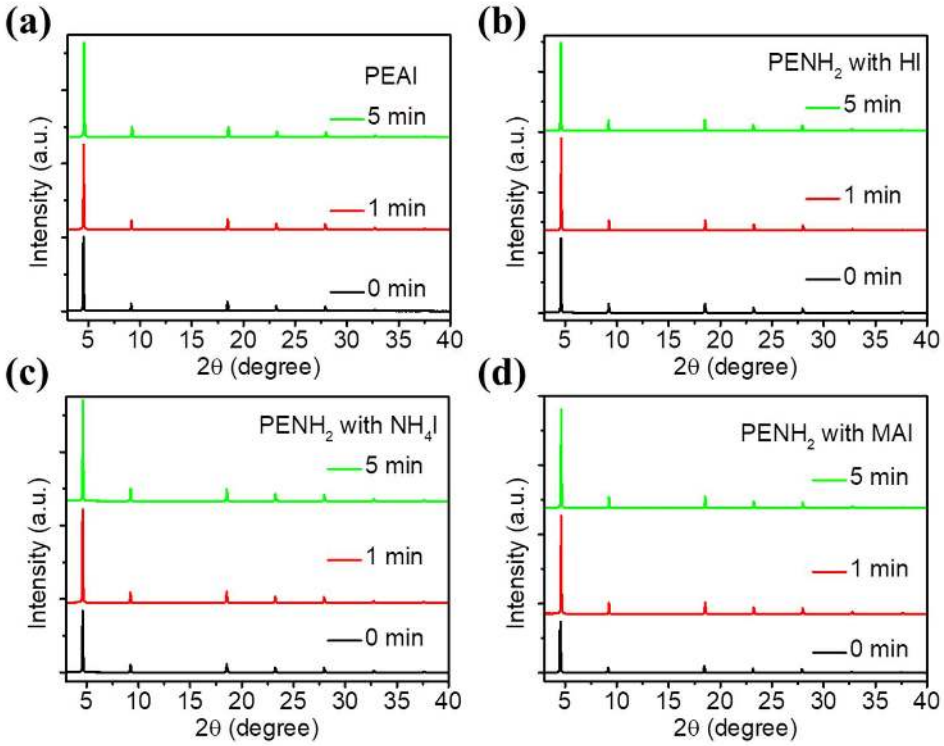

Figure S3. XRD patterns for a) purchased PEAI and films from solutions of $PENH_2$ with b) HI, c) NH_4I or d) MAI annealed at 100 ºC for varied durations.

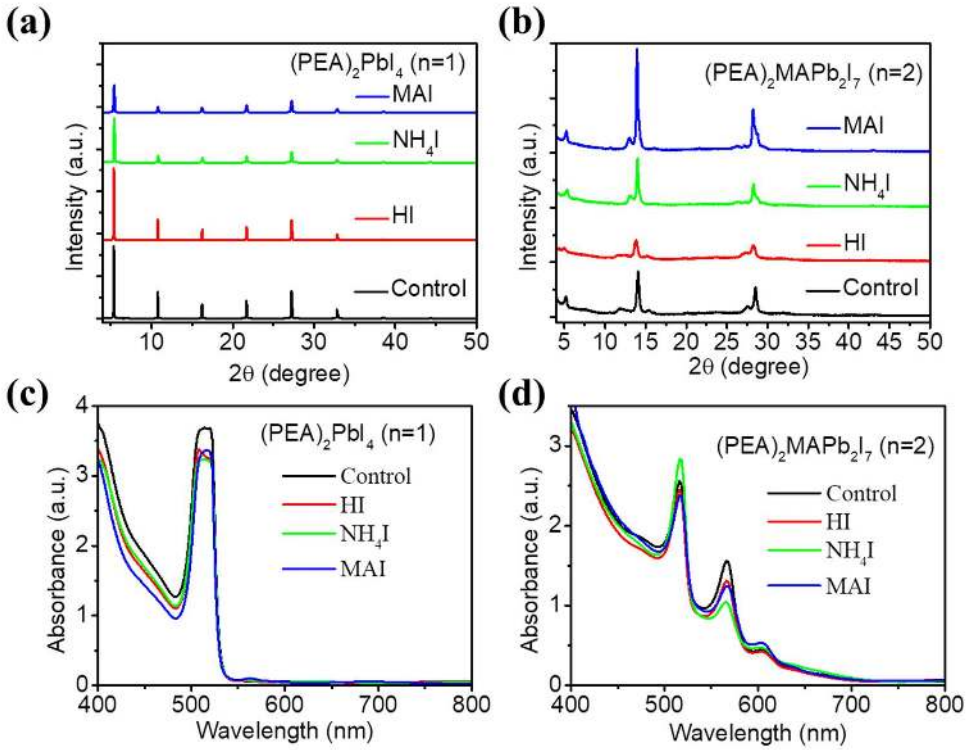

Figure S4. XRD patterns of the RPP films with a) $n = 1$ and b) $n = 2$ from different precursor solutions. c,d) Their corresponding absorption spectra.

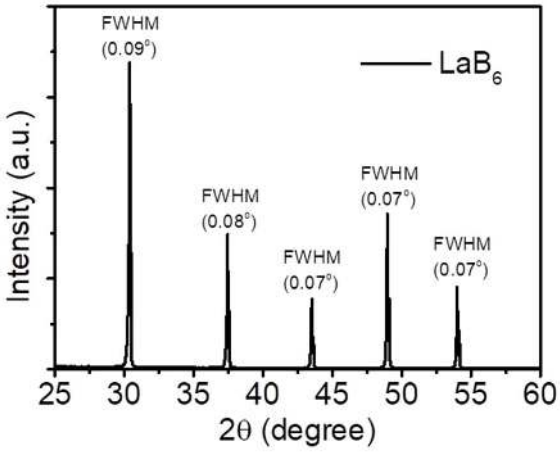

Figure S5. XRD pattern for LaB_6.

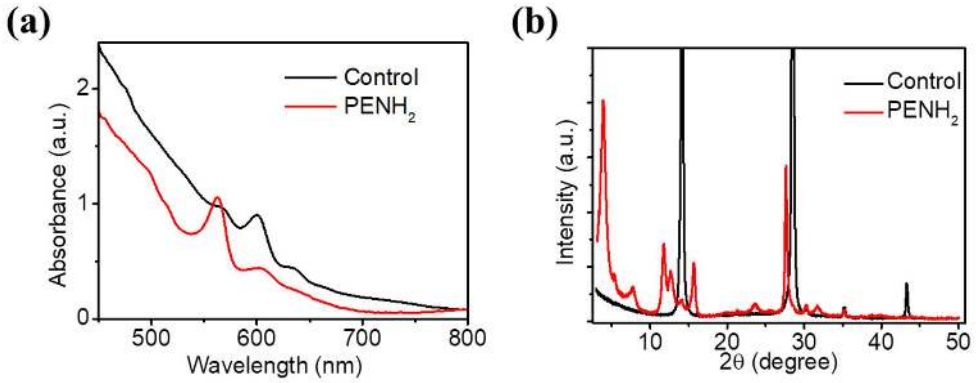

Figure S6. a) Absorption spectra and b) XRD patterns of the RPP film using only $PENH_2$ to replace PEAI as well as the control film for comparison.

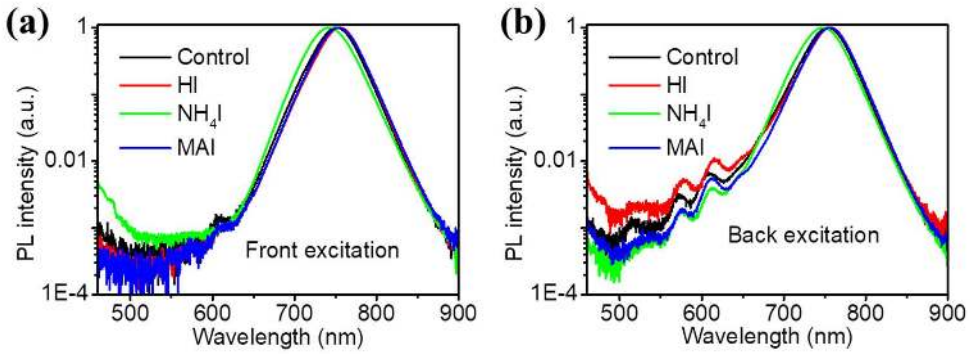

Figure S7. Steady-state PL spectra of the RPP films excited from a) the film side (front excitation) and b) substrate side (back excitation).

Table S1. Transient PL decay parameters of the RPP films (detected at 755 nm).

Sample	A_1 (%)[a]	τ_1 (ns)	A_2 (%)	τ_2 (ns)	τ_{ave} (ns)[b]
control	78.18	13.9±0.6	21.82	80±10	51±3
HI	39.46	5.8±0.9	60.54	27.2±0.9	25±1
NH_4I	30.34	2.9±0.5	69.66	29.4±0.6	29±1
MAI	64.40	9.5±0.5	35.60	79±5	66±3

[a]The curves were fitted using a bi-exponential function $I(t) = A_1\exp(-t/\tau_1) + A_2\exp(-t/\tau_2)$. [b]The average lifetimes (τ_{ave}) are estimated by using the equation of $\tau_{ave} = \sum A_i\tau_i^2/\sum A_i\tau_i$.

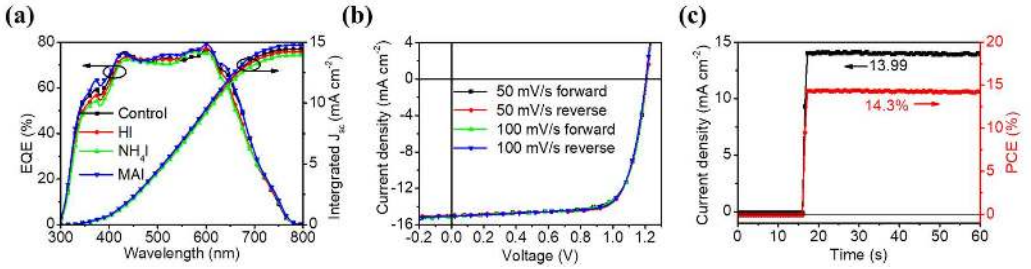

Figure S8. a) Corresponding EQE and integrated J_{SC} of the devices. b) *J–V* curves of a representative device at different scan directions and scan rates and c) steady measurement at the maximum power output point of 1.02 V for the best MAI-based device.

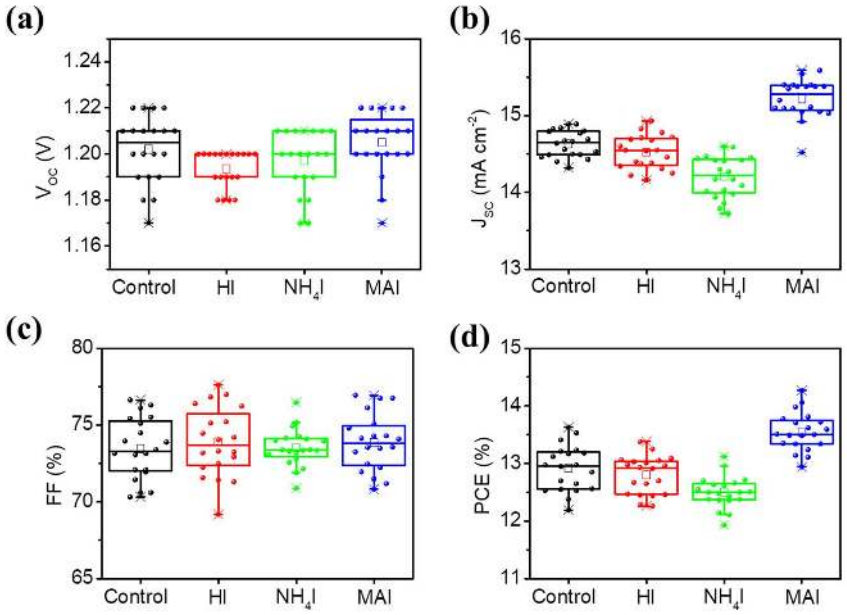

Figure S9. Statistical distribution of photovoltaic parameters for devices from different precursor solutions: a) V_{OC}, b) J_{SC}, c) FF and d) PCE.

Table S2. Statistical device performance parameters of the RPP devices from different precursor solutions.

Devices	V_{OC} (V)	J_{SC} (mA cm^{-2})	FF (%)	PCE (%)
Control	1.20 ± 0.02	14.6 ± 0.2	73.5 ± 2.0	12.9 ± 0.4
HI	1.19 ± 0.01	14.5 ± 0.2	73.9 ± 2.2	12.8 ± 0.3
NH_4I	1.20 ± 0.01	14.2± 0.3	73.5 ± 1.2	12.5 ± 0.3
MAI	1.21 ± 0.01	15.2 ± 0.3	73.9 ± 1.9	13.5 ± 0.3

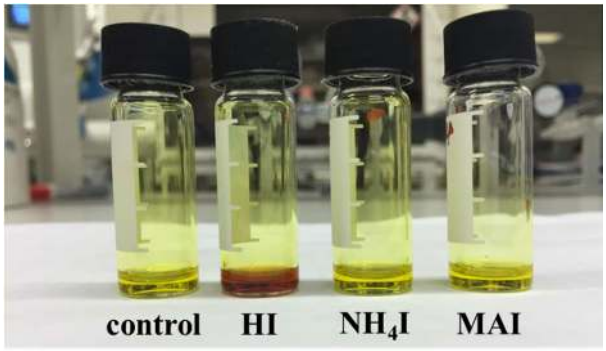

Figure S10. Photographs of the control, HI-, NH_4I-, and MAI-based RPP precursor solutions.

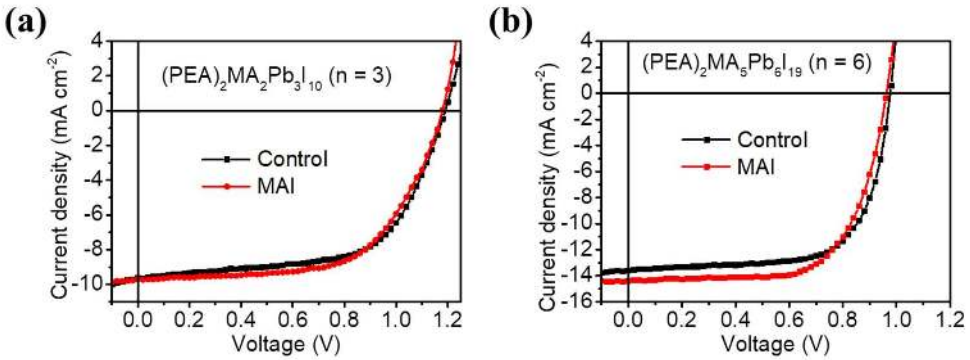

Figure S11. *J–V* curves of solar cells from the control and MAI-based RPP precursor solutions. a) RPP with n = 3, b) RPP with n = 6.

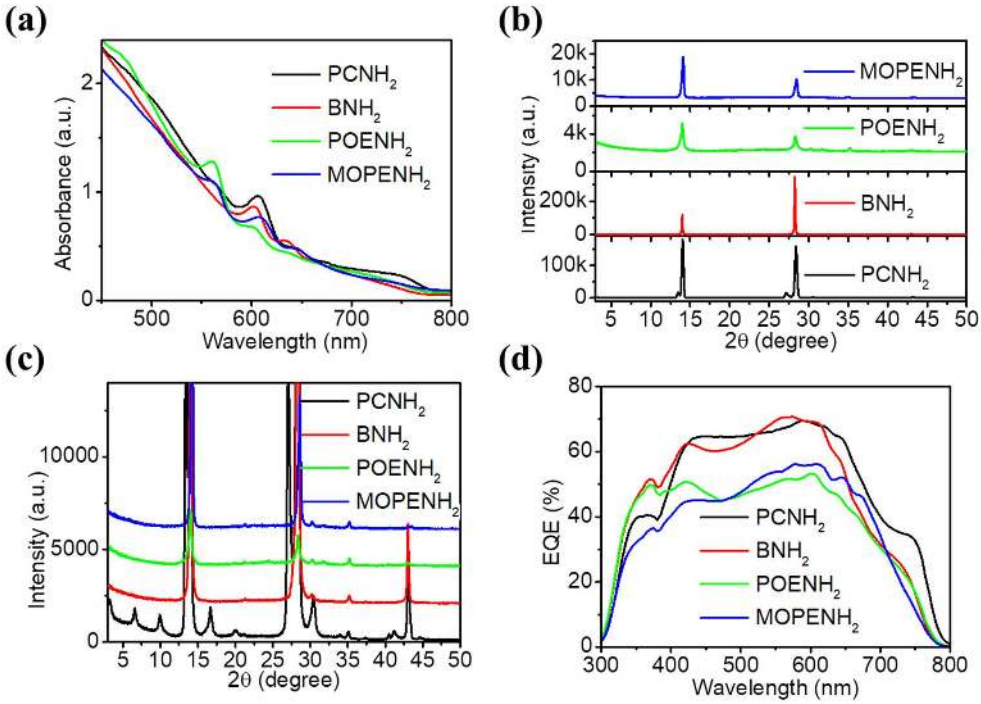

Figure S12. a) Absorption spectra, b) overall XRD patterns and c) XRD patterns with low-intensity peaks of RPP films processed from the four RNH_2-based precursor solutions. d) EQE spectra of the four RNH_2-based RPP solar cells.

Table S3. Photovoltaic parameters of the four RNH_2-based RPP solar cells.

Devices	V_{OC} (V)	J_{SC} (mA cm^{-2})	FF (%)	PCE (%)
$PCNH_2$	1.14	14.6	68.0	11.3
BNH_2	0.98	13.5	76.9	10.2
$POENH_2$	1.18	10.8	69.3	8.8
$MOPENH_2$	0.96	11.2	73.0	7.8

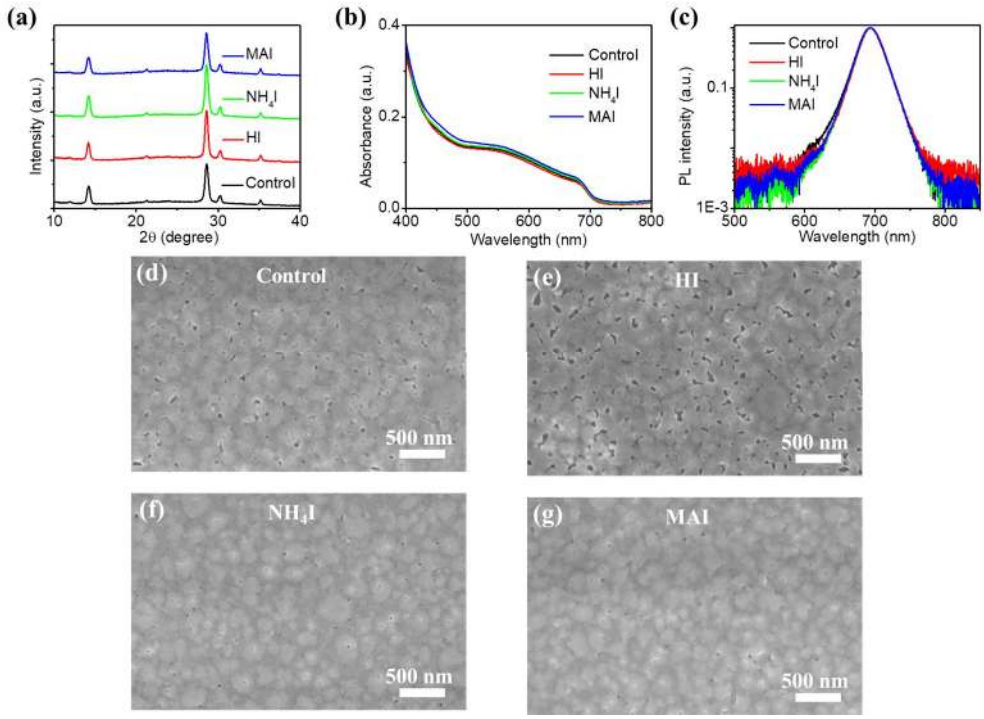

Figure S13. a) XRD patterns, b) absorption spectra and c) Steady-state PL spectra of the NCPI films from different precursor solutions. d–g) SEM images of the NCPI films from d) the control, e) HI-, f) NH_4I-, and g) MAI-based precursor solutions.

Reference

[1] J. Chang, S. Zhang, N. Wang, Y. Sun, Y. Wei, R. Li, C. Yi, J. Wang, W. Huang, *J. Phys. Chem. Lett.* **2018**, *9*, 881.